RSC Advances

PAPER

View Article Online
View Journal | View Issue

Cite this: *RSC Adv.*, 2019, **9**, 6890

Facile synthesis of polypyrrole nanofiber (PPyNF)/NiO_x composites by a microwave method and application in supercapacitors

Huijun Liu, Qiang Zhao, Kewei Wang, Zhen Lu, Feng Feng * and Yong Guo *

In this study, polypyrrole nanofiber (PPyNF)/NiO_x composites were synthesized by a simple and fast microwave method. The samples were characterized using differential scanning calorimetry and thermal gravimetric analysis (DSC/TGA), X-ray photoelectron spectroscopy (XPS) and scanning electron microscopy (SEM). Furthermore, the synthesized PPyNF/NiO_x nanocomposites were electrochemically characterized using galvanostatic charge–discharge, cyclic voltammetry and electrochemical impedance spectroscopy (EIS) techniques. They showed the highest specific capacitance of 657 F g^{-1} at 0.5 A g^{-1}, demonstrating their potential application in supercapacitors.

Received 24th November 2018
Accepted 14th February 2019

DOI: 10.1039/c8ra09666j

rsc.li/rsc-advances

1. Introduction

Supercapacitors are high-capacity devices that are considered promising candidates in energy storage, owing to their higher energy density than conventional capacitors and larger power density than batteries.[1–4] The core of supercapacitors is the electrode material, which directly dominates the performance of energy storage. Among the electroactive materials used for supercapacitors, nickel oxide (NiO) has been identified as an influential candidate because of its high theoretical specific capacitance, high electrochemical stability and excellent redox activities.[5–9] Unfortunately, its practical applications have been limited by its short charge–discharge cycle life. To overcome this shortcoming, scientists have studied the fabrication of nanohybrid materials by integrating conducting polymers (CPs), to improve the cyclability compared with pristine metal oxides.[10–12] For example, Ji *et al.* synthesised polypyrrole/flower-like porous NiO nanocomposites, which exhibits a remarkable cycling stability and shows a capacitance of 595 F g^{-1}, with perfect cycling life (capacitance loss is less than 20% after 1000 cycles).[13] Another important work had been conducted by Cai *et al.*, who fabricated polyaniline (PANI)/nano-NiO nanocomposite by hydrothermal method with β-cyclodextrin as a template. The composite processed a high specific capacitance (2122.75 F g^{-1} at 0.1 A g^{-1} in 0.05 M KI electrolyte solution) and excellent cycle performance (86% capacitance retention after 1000 cycles at 1.5 A g^{-1}).[14] Furthermore, researchers determined that the nanostructure and morphology of conducting polymers, such as nanotube, nanospheres, nanofiber, flower-like and core–shell structures, significantly influence electrochemical properties.[15–17] For instance, Wang *et al.* prepared PANI@multiwall carbon nanotube (MWCNT) hybrid films through *in situ* electrochemistry, producing PANI nanowires with a diameter of 8 nm confined within a 10 nm-diameter MWCNT porous membrane; the membranes exhibited a good electrochemical capacitance of 296 F g^{-1} with a capacitance retention of 95% after 2000 cycles.[18] Li *et al.* proposed a polyaniline/polypyrrole (PANI/PPy) composite nanofibers with core–shell structures electrode for supercapacitor applications. The composite nanofibers showed the highest specific capacitance of 834.6 F g^{-1} at the scan rate of 5 mV s^{-1}.[19] Another similar research has been reported by Cai's group, as active electrode materials, graphene nanosheet and PPy nanotube nanocomposite show a highest specific capacitance of 368 F g^{-1} with an excellent capacitive retention of 91.4% after 1000 cycles.[20] These results indicate that the nanostructure of CP composites exhibit potential in the development of high-performance electrode materials.

The most commonly used conducting polymers include polypyrrole (PPy), polyaniline (PANI) and their derivatives.[21–23]

College of Chemistry and Environmental Engineering, The University of Shanxi Datong, Datong, 037009, P. R. China

Table 1 Raw material list and reaction conditions for synthesizing PPyNF/NiO_x composites

Sample	P^a : N^b	P^a (mg)	N^b (mg)	Microwave power (W)	Heating time (s)
a	50 : 30	50	30	800	60
b	50 : 40	50	40	800	60
c	50 : 50	50	50	800	60
d	50 : 40	50	40	600	60
e	50 : 40	50	40	1000	60
f	50 : 40	50	40	800	30
g	50 : 40	50	40	800	90

[a] Mass of polypyrrole nanofiber. [b] Mass of $Ni(NO_3)_2 \cdot 6H_2O$.

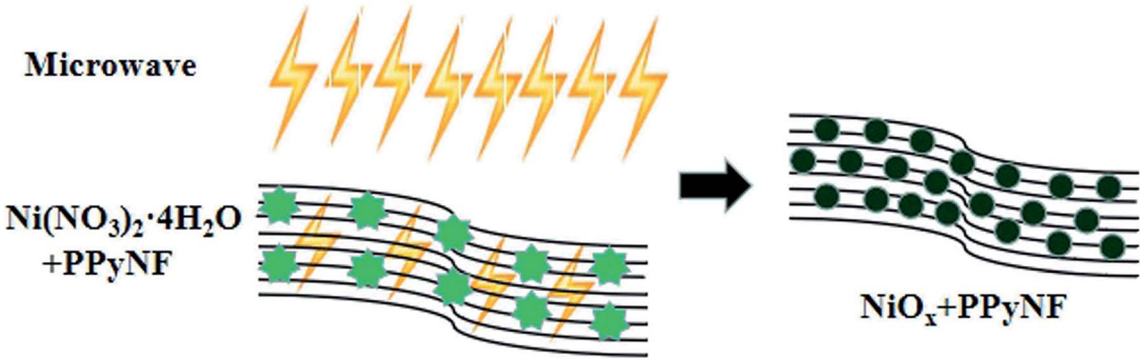

Scheme 1 The mechanism of (PPyNF)/NiO composites was prepared by microwave.

In recent years, PPy composites have been widely used in supercapacitors due to their electrochemical stability, high conductivity (10–100 S cm^{-1}) and intrinsic flexibility;[24–26] PPy also possesses better electronic and electrochemical properties compared with PANI. In this study, facile and energy efficient microwave assisted solid-state synthesis of PPy/NiO_x nanocomposite was reported. The synthesised samples were further electrochemically investigated for their performance as potential supercapacitors.

2. Experimental

2.1. Materials

All the chemicals purchased were reagent grade. Nickel nitrate hexahydrate ($Ni(NO_3)_2 \cdot 6H_2O$, 98.5%), ferric chloride ($FeCl_3$), potassium hydroxide (KOH) and pyrrole (Py) were obtained from Aladdin Industrial Corporation (Aladdin Reagent Co., Ltd.), Shanghai, China. All aqueous solutions were prepared in deionized water (18.2 MΩ cm of resistivity at 25 °C).

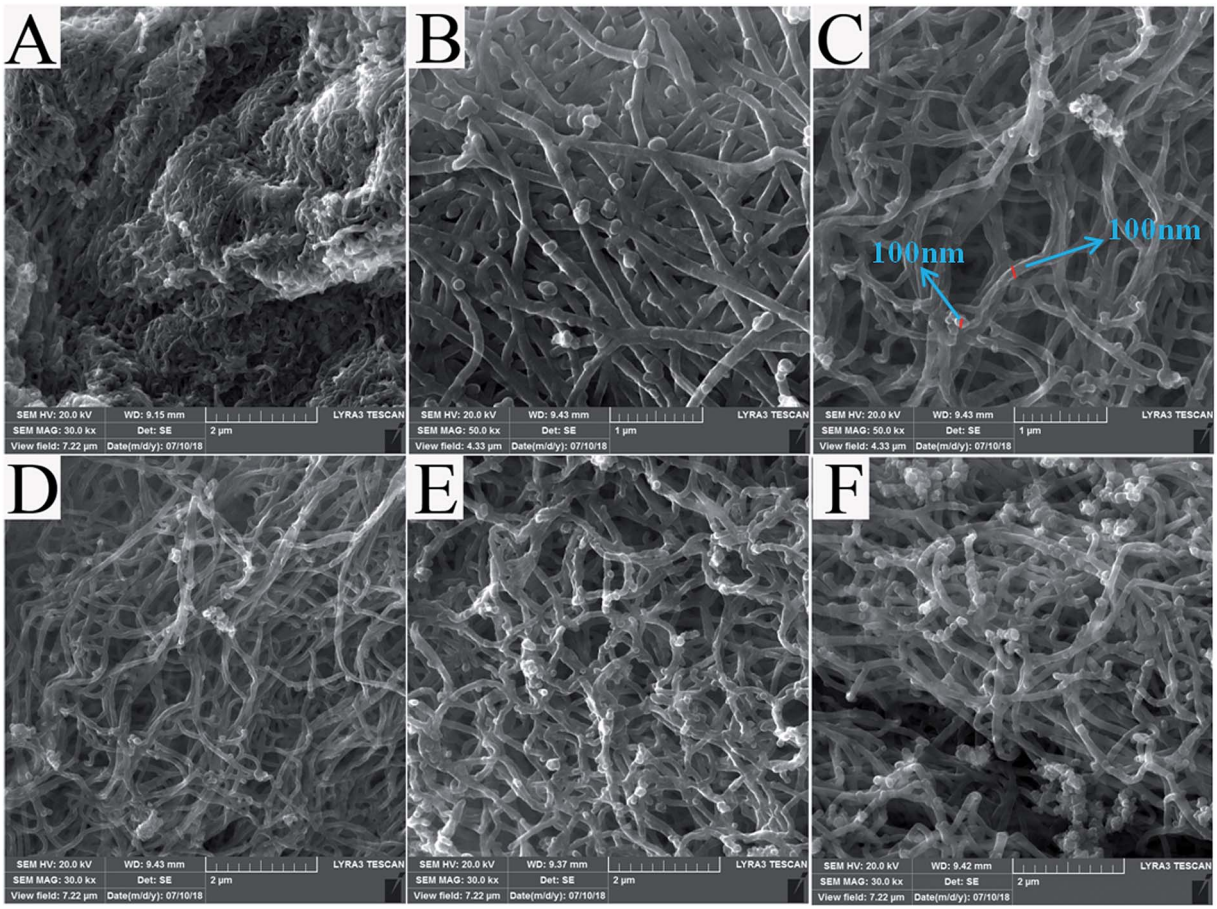

Fig. 1 SEM images of as-prepared samples (A) and (B) PPyNF and (C)–(E) and (F) PPyNF–NiO_x nanocomposite.

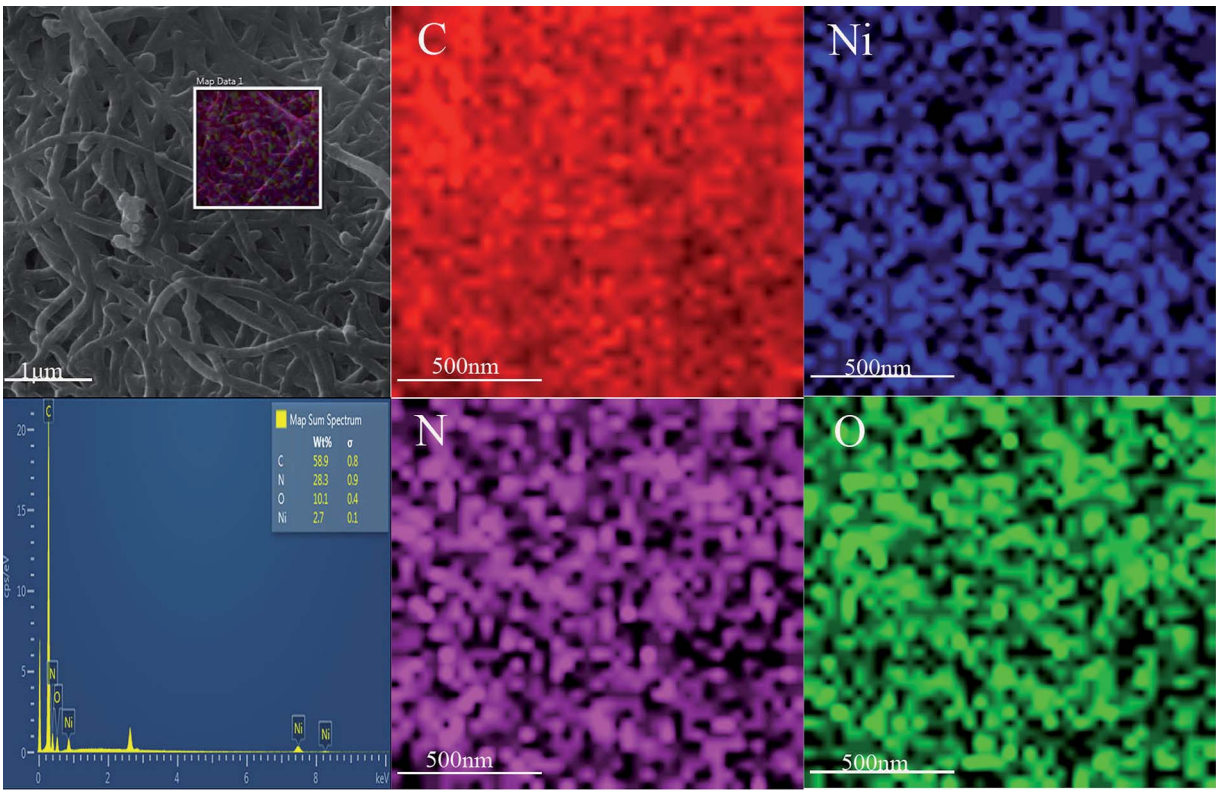

Fig. 2 EDS mapping of PPyNF–NiO_x nanocomposite.

2.2. Preparation of PPyNF

The polypyrrole nanofiber (PPyNF) was synthesized from V_2O_5 nanofibers and pyrrole according to the literature.[27] Pyrrole (1 mL) were dissolved in 1 M HCl solution (60 mL), and then, a certain amount of V_2O_5 nanofibers (1–2 mL) were added. After stirring for 20 minutes, APS solution (1 g APS dissolved in 20 mL 1 M HCl) was added to the above solution. Under magnetic stirring for 20 minutes at 25 °C, the resulting suspension was filtered and washed several times with deionized water and acetone until filtrate was colorless. Finally, it was vacuum dried at 80 °C for 12 h.

2.3. Preparation of PPyNF/NiO_x nanocomposites

The PPyNF/NiO_x nanocomposites were prepared through a facile and ultrafast microwave solid-state approach. In a typical procedure, 40 mg $Ni(NO_3)_2 \cdot 6H_2O$ as metal precursor and 50 mg PPyNF as thermal conductivity layer were mixed to each other and finely powdered in an agate mortar. The PPyNF was used as the microwave absorbing material and heating layer to facilitate the decomposition of $Ni(NO_3)_2 \cdot 6H_2O$. This leads to the formation of NiO_x nanocomposites under microwave irradiation due to the strong microwave absorption of PPyNF.[8] The mechanism of formation of the PPyNF/NiO_x nanocomposites is schematically shown in Scheme 1. Subsequently, the mixture was transferred to an alumina crucible and put into a domestic microwave oven (PANASONIC NN-GF352M, 2450 MHz, 1000 W) with a power of 800 W for 60 s. After a while, the powder of PPyNF/NiO nanocomposite were collected. The other PPyNF/NiO_x nanocomposite of different material ratios, microwave radiation time and power were also prepared. All the related information is given in Table 1.

2.4. Characterization

Thermal gravimetric analysis (TGA) measurement and Differential scanning calorimetric (DSC) analyses were performed using a Netzsch STA 449C (Germany) with a heating rate of 10 °C min^{-1} and temperature ranging from 30 °C to 1000 °C under nitrogen atmosphere. X-ray diffraction (XRD) patterns

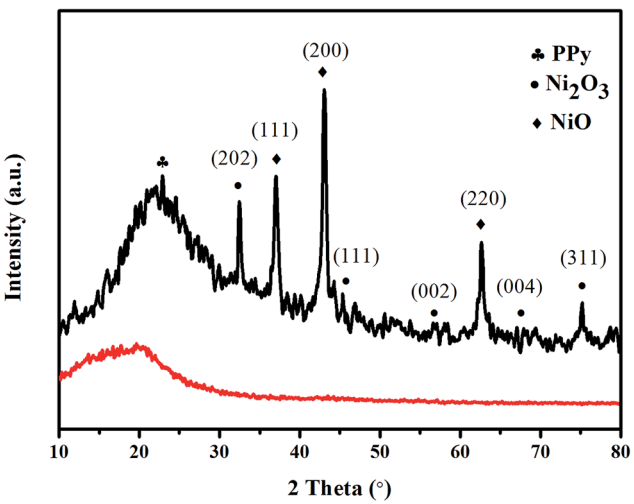

Fig. 3 XRD spectra of PPyNF and PPyNF–NiO_x nanocomposites.

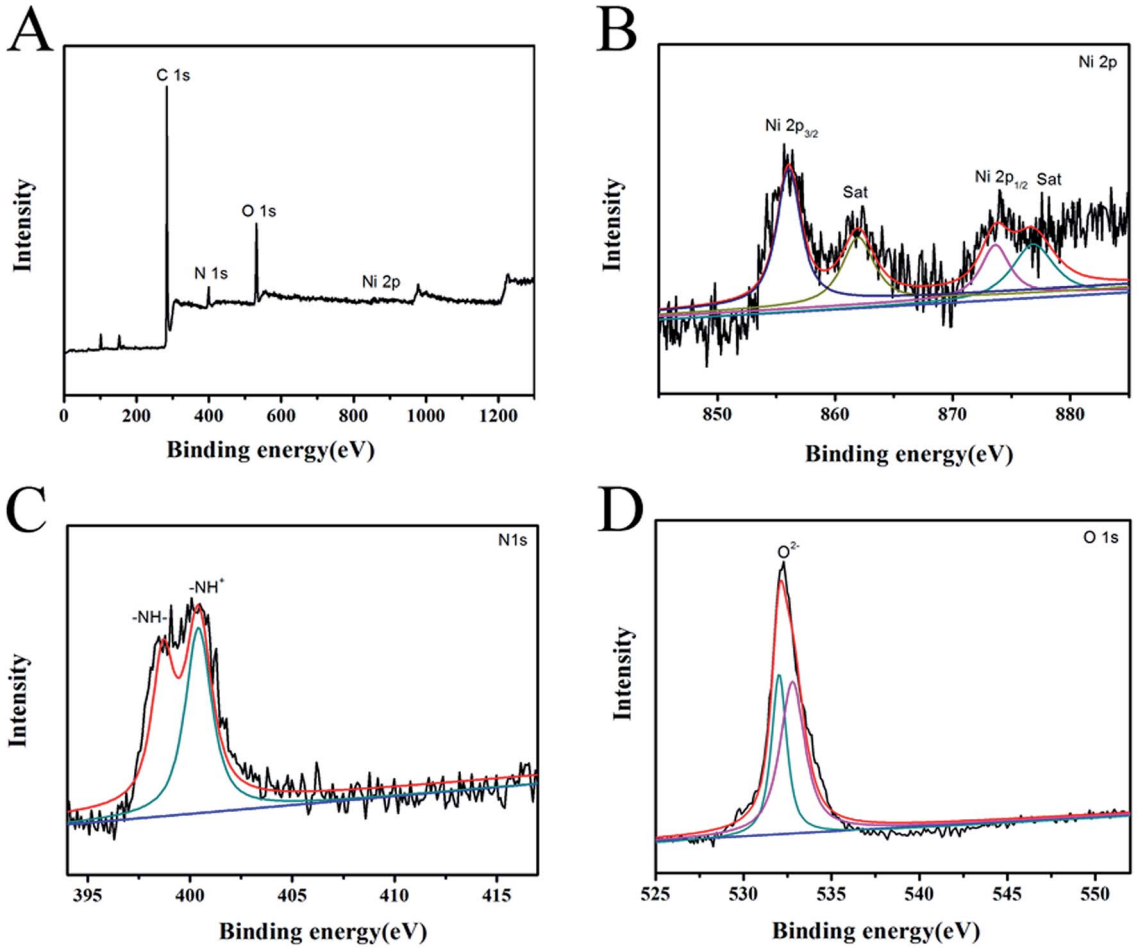

Fig. 4 XPS spectra of PPyNF–NiO_x nanocomposites (A) survey spectrum, (B) Ni 2p, (C) N 1s, (D) O 1s.

with Cu target (36 kV, 25 mA) were performed in 2θ range from 5° to 60°, with a step size of 0.02° and a scanning speed of 8° min^{-1}. Scanning electron microscopy (SEM) of the samples was analyzed using KYKY-EM3800. All electrochemical measurements (ChenHua CHI660E) were evaluated in single compartment three-electrode electrochemical cell containing 6 M KOH as an electrolyte. The working electrode was prepared by mixing as-synthesized PPy/NiO_x nanocomposites (active materials) with acetylene black (conductive agent) and polyvinylidene fluoride (PVDF, binder) in a 80 : 10 : 10 weight ratio using *N*-methyl-2-pyrrolidone (NMP) as a solvent to make a homogeneous slurry. After smeared the slurry into a Ni foam (1×1 cm^2) current collector, the Ni foam with slurry was dried at 80 °C for 24 h and then pressed under a pressure of 10 MPa. The loading mass of active material was approximately 0.72 mg cm^{-2}. Correspondingly, the platinum (Pt) foil and mercury/mercury oxide electrode (Hg/HgO) were used as the counter electrode and a reference electrode, respectively.

3. Results and discussion

3.1. Synthesis and characterization

The SEM images of PPyNF and PPyNF/NiO_x nanocomposites were shown in Fig. 1A–F, respectively. Fig. 1A and B show the SEM images of PPyNFs, which were approximately 100 nm in diameter and 5000 nm in length. Likewise, Fig. 1C–F show the SEM images of PPyNF/NiO_x nanocomposites, where nanoparticle structured NiO_x was observed, where a mass of NiO_x nanoparticles were grown intricately on the surface of PPyNFs. The average diameter of nanoparticles was found to be about 100 nm. The lower microwave power, 600 W, yields a lower

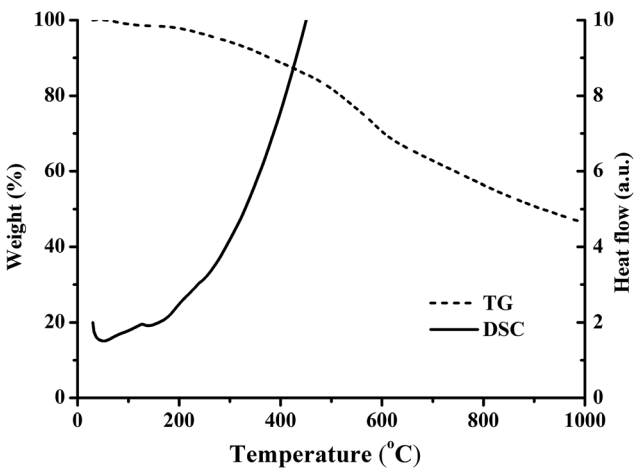

Fig. 5 TGA-DSC spectra of PPyNF–NiO_x nanocomposites.

amount of product compared to the higher microwave power, 800 W (in Fig. 1D and E). Additionally, the higher microwave (1000 W) power may affect the NiO_x particles, making agglomeration (in Fig. 1E and F). The purity of synthesized PPyNF/NiO_x nanocomposites was suggested by EDS spectra shown in Fig. 2, where C, N, Ni and O were detected. Fig. 3 presents the XRD patterns of PPyNF/NiO_x composite. PPyNF revealed a sharp and intense diffraction peak located at 21. For PPyNF/NiO_x composite, the diffraction peaks at 36.78°, 42.92° and 62.4°, which can be assigned to the (111), (200) and (220) reflections of NiO, respectively, as per the JCPDS PDF# 78-0643. Diffraction peaks were also observed at 2θ degrees of 31.67°, 45.42°, 56.43°, 66.19° and 75.26°, which can be attributed to the (202), (111), (002), (004) and (311) reflections of Ni_2O_3 as per the JCPDS PDF# 14-0481 ref. 28, respectively. These XRD results indicate that NiO_x was a mixture of NiO and Ni_2O_3. The oxidation states of NiO_x nanoparticles were also determined by XPS (Fig. 4). The full survey scan spectrum (Fig. 4A) shows the peaks of four elements (C, N, Ni, and O). As shown in Fig. 4B, in the spectrum of Ni 2p, the major peaks at 856.2 and 874 eV correspond to the Ni 2p3/2 and Ni 2p1/2 spin orbit levels, respectively. The binding energy gap between Ni 2p3/2 and Ni 2p1/2 approached 17.8 eV, indicating that the nanocomposite contains Ni^{2+} and Ni^{3+}. Two similar peaks were noted at 398 and 399.4 eV, which were identified in the N1s spectrum in Fig. 4C and assigned to neutral amine nitrogen and amine nitrogen (N^+) within the PPy, respectively.[29] The O 1s spectrum is single peaks at 532.5 eV (Fig. 4D), which belong to O^{2-} forming oxides with Ni. Fig. 5 shows the TGA-DSC spectra of PPyNF–NiO_x nanocomposites from RT to 1000 °C. The PPyNF–NiO_x nanocomposites exhibited a three-step thermal degradation. The initial weight loss, which is approximately 100–250 °C, was mainly due to the evaporation of moisture. The second weight loss, which is approximately 350–600 °C, was attributed to the decomposition of NiO_x. The final weight loss, which was approximately 600–1000 °C, was caused by the generalized PPy backbone degradation. DSC spectra shows clear transition around 160 °C. Here, the upper peak indicates that the material absorbs more heat as compared to the reference sample which corresponds to the exothermic transition of the material.

3.2. Electrochemical performance

To determine the optimal preparation conditions, we have tested the electrochemical properties of samples a–g and showed their specific capacitances at different current densities in Fig. 6. As shown in Fig. 6A, the specific capacitance of PPyNF/NiO_x electrode presented an increase-and-decrease trend with increasing $Ni(NO_3)_2 \cdot 6H_2O$. With $Ni(NO_3)_2 \cdot 6H_2O$ mass ranging

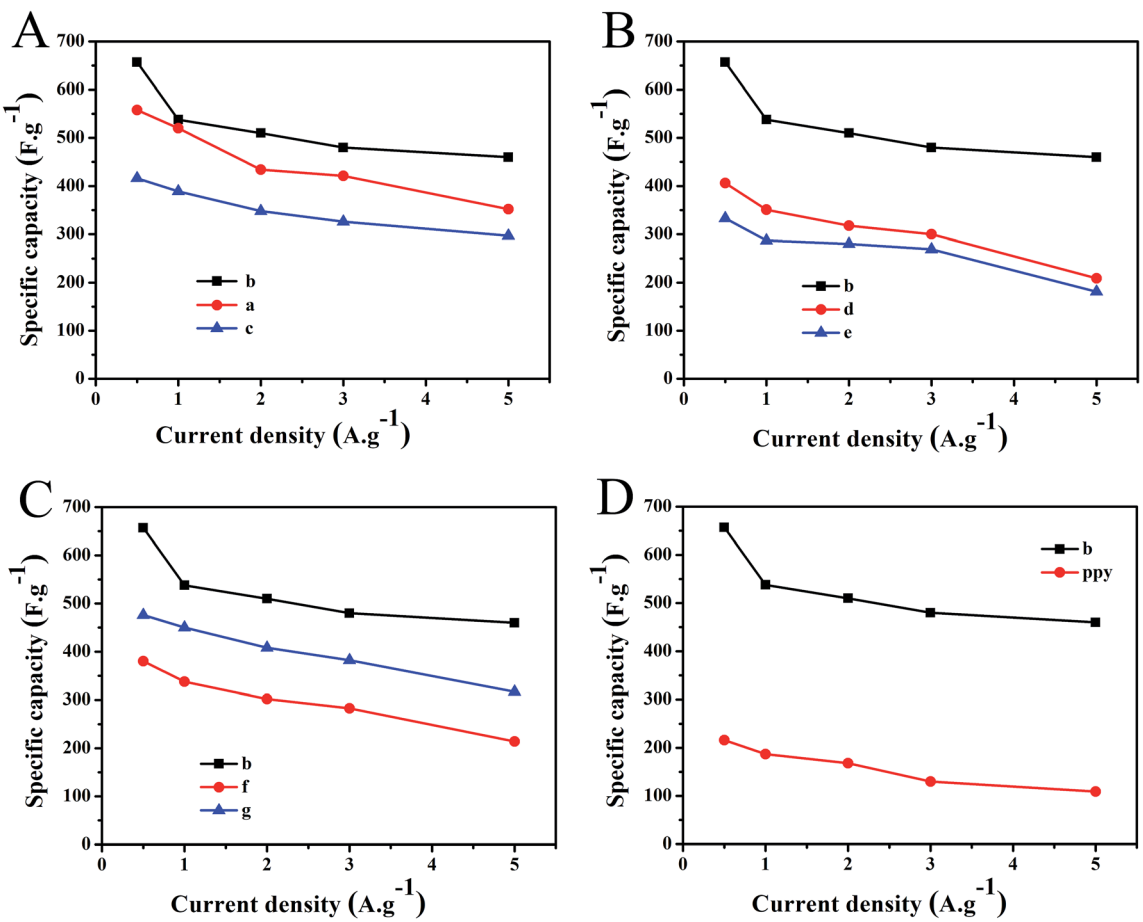

Fig. 6 Specific capacity of PPyNF–NiO_x nanocomposite at different current density (A) sample a–c, (B) sample b–e, (C) sample b–g, (D) sample b and PPy.

from 30 mg to 40 mg, the content of NiO_x generated increased and the specific capacitance increased gradually. However, when $Ni(NO_3)_2 \cdot 6H_2O$ mass increased to 50 mg, the content of crystallinity water of the precursor could not be ignored. When the content of crystallinity water is too high, the microwave energy absorbed by PPyNF becomes insufficient, and the precursor cannot be completely decomposed, leading to decreases in the electrochemical properties of the nanocomposite. For instance, the specific capacitance of sample b reached 657 F g^{-1} at 0.5 A g^{-1}, which was higher than those of samples a and c. The effect of microwave time and microwave power on special capacitors have been shown in Fig. 6B and C. It can be seen from Fig. 6B and C, when the reaction time is 60 s and the microwave power is 800 W, sample b showed the best special capacitor. Extremely low microwave power or considerably short reaction time will lead to insufficient microwave energy absorbed by the heating layer, and the precursor cannot be completely decomposed, whereas extremely high microwave power or notably long reaction time will affect the growth of NiO_x particles. For example, the specific capacitance of sample b was higher than those of samples d and e. As shown in Fig. 1D–F, the lower microwave power yields a lower amount of product and the higher microwave power may affect the NiO_x particles, making agglomeration. Thus, the optimum experimental conditions for synthesis of PPyNF/NiO_x nanocomposite include a 50 : 40 mass ratio, 800 W microwave power and 60 s microwave time. The specific capacitances are 657, 538, 510, 480 and 460 F g^{-1}at the current densities of 0.5, 1, 2, 3 and 5 A g^{-1}, respectively, showing the rate capability of the synthesized sample b (Fig. 6D).

The electrochemical performance of PPyNF/NiO_x nanocomposite of sample b was investigated by cyclic voltammetry (CV), galvanostatic charge/discharge (GCD), and electrochemical impedance spectroscopy (EIS) measurements. As shown in Fig. 7A, the CV curves of PPyNF/NiO_x showed a pair of well-defined redox peaks at all scan rates, which were due to the reversible faradaic redox reaction between Ni^{2+} and Ni^{3+}. This process might be represented by the following equation:[30]

$$Ni(II)_S + OH^- \leftrightarrow Ni(II)OH_{ad} + e^-$$

With the increase in scan rate, the anodic and cathodic peak potentials shifted in more positive and negative directions, respectively, causing no significant change in the shape of CV curves. This finding indicates the good rate capability of PPyNF/NiO_x. The pseudocapacitance behaviour was also observed in the GCD curves of PPyNF/NiO_x electrode within a potential window of 0–0.5 V at all current densities (Fig. 7B). To further characterise the performance of the supercapacitors, the long-term cycle stability of the electrodes was examined by

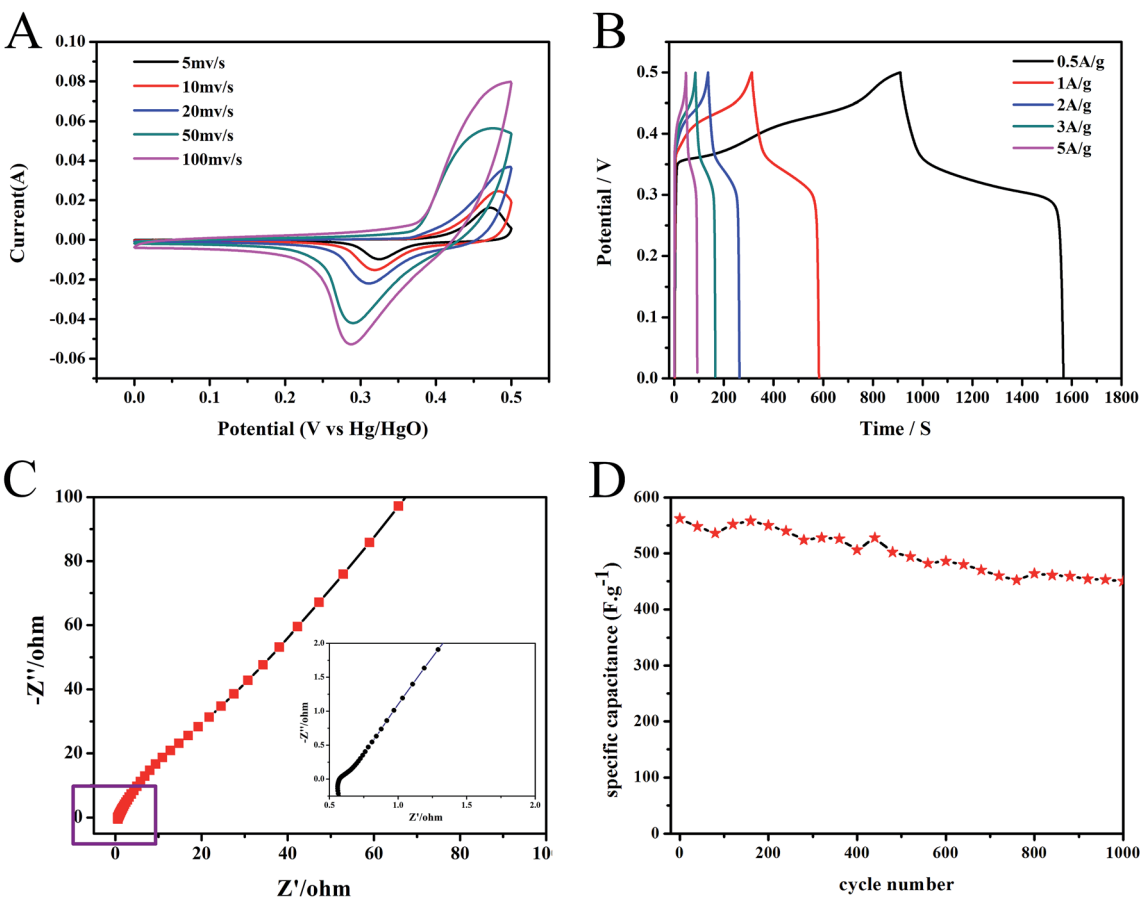

Fig. 7 (A) CV curves of sample b with varied scan rates, (B) GCD curves of sample b at different current densities, (C) cyclability of sample b at 1 A g^{-1}, (D) Nyquist plots of sample b at open circuit potential.

Table 2 Comparison of capacitance of NiO based materials reported recently

Materials	Prepared method	Capacity	Ref.
3D flower-like porous structure NiO@PPy composite	Hydrothermal method	595 F g^{-1} (1 A g^{-1})	13
PANI/nano-NiO composite	Hydrothermal method	2122.75 F g^{-1} (0.1A g^{-1})	14
N-doped porous carbon (NPC)/NiO composites	Liquid oxidation	404 F g^{-1} (1 A g^{-1})	31
Carbon cloth nickel oxide–polyaniline (EC-NiO/PANI)	Hydrothermal method	193 F g^{-1} (0.5 A g^{-1})	32
Polypyrrole nanofiber (PPyNF)/NiO_x composites	Microwave method	657 F g^{-1} (0.5 A g^{-1})	This work

repeated GCD testing at a current density of 1 A g^{-1}, revealing an the excellent cycle life with 80% retention of specific capacitance after 1000 cycles (Fig. 7C). The Nyquist plot of sample b was measured using an AC voltage with 5 mV amplitude with a frequency range of 100 kHz to 0.01 Hz at the open circuit potential. As depicted in Fig. 7D, the small semi-circle at higher frequencies indicates a low charge transfer resistance with slight diffusion at lower frequencies. This result further affirms the excellent electrochemical cycling stability of PPyNF/NiO_x nanocomposite which showed potential application as electrode material for supercapacitors. Table 2 compares the specific capacitance and preparation method between the system of our present work and the reported values. The PPyNF/NiO_x nanocomposites successfully increase the specific capacitance by the simple and fast microwave method. Overall, this study suggests that PPyNF/NiO_x nanocomposites feature a number of advantages over numerous materials when considering various strategies.

4. Conclusions

PPyNF/NiO_x nanocomposite have been successfully synthesized *via* ultrafast microwave irradiation method respectively. The PPyNF/NiO_x nanocomposite showed highest specific capacitance (657 F g^{-1} at a current density of 0.5 A g^{-1}) with mass ratio of 50 : 40 (PPyNF/$Ni(NO_3)_2 \cdot 6H_2O$), microwave heating time of 60 s and microwave power of 800 W. In addition, excellent cycling stability with capacitance retention of 80% of the initial value after 1000 cycles was further investigation at a current density of 1 A g^{-1}. Thus, the PPyNF/NiO_x nanocomposite can be considered to a potential material for energy storage.

Conflicts of interest

There are no conflicts to declare.

Acknowledgements

The authors thank the financial support of the Natural Science Foundation of China (21073113).

References

1 H. Kashani, L. Y. Chen, Y. k. Ito, J. H. Han, A. k. Hirata and M. W. Chen, *Nano Energy*, 2016, **19**, 391–400.
2 A. H. P. Oliveira and H. P. Oliveira, *J. Power Sources*, 2014, **268**, 45–49.
3 S. Chu and A. Majumdar, *Nature*, 2012, **488**, 294–303.
4 C. Liu, F. Li, L. P. Ma and H. M. Cheng, *Adv. Mater.*, 2010, **22**, E28–E62.
5 Y. Mao, Q. Y. Kong, B. k. Guo, L. Shen, Z. X. Wang and L. Q. Chen, *Electrochim. Acta*, 2013, **105**, 162–169.
6 J. W. Lee, T. Ahn, J. H. Kim, J. M. Ko and J. D. Kima, *Electrochim. Acta*, 2011, **56**, 4849–4857.
7 X. M. Wu, Q. G. Wang, W. Z. Zhang, Y. Wang and W. X. Chen, *Electrochim. Acta*, 2016, **211**, 1066–1075.
8 Y. H. Bi, A. Nautiyal, H. P. Zhang, J. J. Luo and X. Y. Zhang, *Electrochim. Acta*, 2018, **260**, 952–958.
9 X. Q. Wang, Q. Q. Li, Y. Zhang, Y. F. Yang, Z. Cao and S. X. Xiong, *Appl. Surf. Sci.*, 2018, **442**, 565–574.
10 B. F. Zhang, P. F. Zhou, Y. L. Xu, J. Lin, H. Li, Y. Bai, J. B. Zhu, S. C. Mao and J. Wang, *Chem. Eng. J.*, 2017, **330**, 1060–1067.
11 Y. C. Zhao and C. A. Wang, *Mater. Des.*, 2016, **97**, 512–518.
12 K. Wang, H. Wu, Y. Meng and Z. X. Wei, *Small*, 2014, **10**, 14–31.
13 W. J. Ji, J. Y. Ji, X. H. Cui, J. J. Chen, D. J. Liu, H. Deng and Q. Fu, *Chem. Commun.*, 2015, **51**, 7669–7672.
14 X. M. Cai, X. G. Cui, L. Zu, Y. Zhang, X. Gao, H. Q. Lian, Y. Liu and X. D. Wang, *Polymers*, 2017, **9**, 288–301.
15 X. Jian, J. G. Li, H. M. Yang, L. L. Cao, E. H. Zhang and Z. H. Liang, *Carbon*, 2017, **114**, 533–543.
16 X. Cai, S. H. Lim, C. K. Poh, L. F. Lai, J. Y. Lin and Z. X. Shen, *J. Power Sources*, 2015, **275**, 298–304.
17 T. Y. Huang, C. W. Kung, H. Y. Wei, M. B. Karunakara, C. W. Chu and K. C. Ho, *J. Mater. Chem. A*, 2014, **2**, 7229–7237.
18 R. R. Wang, Q. Wu, X. H. Zhang, Z. H. Yang, L. J. Gao, J. F. Ni and K. C. T. Ophelia, *J. Mater. Chem. A*, 2016, **4**, 12602–12608.
19 T. Li, Y. Zhou, Z. J. Dou, S. Dong, N. Liu and Z. Y. Qin, *Electrochim. Acta*, 2017, **243**, 228–238.
20 Z. Cai, H. Xiong, Z. Zhu, H. B. Huang, L. Li, Y. N. Huang and X. H. Yu, *Synth. Met.*, 2017, **227**, 100–105.
21 H. Wei, C. He, J. Liu, H. B. Gu, Y. R. Wang, X. R. Yan, J. Guo, D. W. Ding, N. Z. Shen, X. F. Wang and S. Y. Wei, *Polymer*, 2015, **67**, 192–199.
22 X. Wang, L. Jia, Q. Liu, J. Y. Liu, X. F. Guo, X. Y. Jing and J. Wang, *Colloids Surf., A*, 2016, **506**, 646–653.
23 G. A. Snook, P. Kao and A. S. Best, *J. Power Sources*, 2011, **196**, 1–12.
24 G. F. Chen, Z. Q. Liu, J. M. Lin, N. Li and Y. Z. Su, *J. Power Sources*, 2015, **283**, 484–493.
25 Y. F. Zhu, F. F. Wang, H. L. Zhang, X. B. Lv, Z. F. Hu, H. Han, X. Y. Fan, J. Y. Ji and X. D. Guo, *J. Alloys Compd.*, 2018, **747**, 276–282.

26 X. M. Wu, L. Meng, Q. Q. Wang, W. Z. Zhang and Y. Wang, *Chem. Eng. J.*, 2017, **327**, 193–201.
27 Y. X. Zhang and S. K. Manohar, *J. Am. Chem. Soc.*, 2004, **126**, 12714–12715.
28 M. Shaban, M. R. Abukhadra, A. Hamd, R. R. Amin and A. A. Khalek, *J. Environ. Manage.*, 2017, **204**, 189–199.
29 Y. Chu, S. Xiong, B. Li, Y. T. Qian and B. J. Xi, *ChemElectroChem*, 2016, **3**, 1347–1353.
30 Y. Jiao, Y. Liu, B. Yin, S. W. Zhang, F. Y. Qu and X. Wu, *Nano Energy*, 2014, **10**, 90–98.
31 X. Q. Wang, Q. Q. Li, Y. Zhang, Y. F. Yang, Z. Cao and S. X. Xiong, *Appl. Surf. Sci.*, 2018, **442**, 565–574.
32 S. A. Razali and S. R. Majid, *Mater. Des.*, 2018, **153**, 24–35.